Journal of The Electrochemical Society, **158** (8) A976-A981 (2011)
0013-4651/2011/158(8)/A976/6/$28.00 © The Electrochemical Society

A Comparative Study of Electrochemical Capacitive Behavior of $NiFe_2O_4$ Synthesized by Different Routes

Shahid Anwar,[a] K. Sudalai Muthu,[a] V. Ganesh,[b,z] and N. Lakshminarasimhan[c,*,z]

[a]Central Instrumentation Facility Division, [b]Electrodics and Electrocatalysis Division, and [c]Functional Materials Division, CSIR-Central Electrochemical Research Institute, Karaikudi-630006, Tamil Nadu, India.

The electrochemical capacitive behavior of $NiFe_2O_4$ ceramic powders prepared by combustion synthesis, polyol-mediated and sol-gel methods was studied. The phase formation and morphological characterizations of synthesized materials were carried out through thermal analysis (TG-DTA), powder X-ray diffraction (XRD) and scanning electron microscopy (SEM). Electrochemical performance of these electrode materials as capacitors was investigated in aqueous NaCl electrolyte using cyclic voltammetry (CV) and the corresponding specific capacitance (SC) values were determined. The observed electrochemical double layer capacitive (EDLC) behavior in $NiFe_2O_4$ depends on the morphology which can be controlled by the synthesis method adopted. $NiFe_2O_4$ synthesized by sol-gel method exhibited a specific capacitance of 97.5 F/g which is higher than the capacitance values of $NiFe_2O_4$ obtained through other synthesis methods.
 [DOI: 10.1149/1.3601863]

Manuscript submitted March 24, 2011; revised manuscript received May 24, 2011. Published June 23, 2011.

Electrochemical capacitors (EC) receive a great deal of research attention in recent years in the field of energy storage and conversion due to their promising properties.[1–5] Complementary to battery, ECs can provide superior power density and cyclability, and can be regarded as an intermediate device between the traditional ceramic capacitors and batteries.[2] ECs can be used for power enhancement and cycle life improvement of power sources such as batteries and fuel cells. Much research has been focused towards the development of materials for capacitor applications.[6] Carbon in different forms finds suitable application as electrochemical double layer capacitors (EDLCs) due to its high specific surface area, good intra- and inter-particle conductivity.[7] However, accessibility of the electrolyte at the porous surface of carbon limits its use and makes it necessary to explore metal oxide based capacitors. Although hydrated amorphous ruthenium oxide, $RuO_2{\cdot}xH_2O$, is well known for its high specific capacitance and power-density in aqueous H_2SO_4, its commercial applications are limited due to higher cost.[8–10] In this direction, low cost amorphous $MnO_2.xH_2O$ was shown to exhibit a comparable supercapacitor behavior in aqueous KCl electrolyte (mild conditions) to that of $RuO_2{\cdot}xH_2O$ in acidic condition (H_2SO_4).[11] Nickel containing oxides with high surface area have also been demonstrated as capacitors due to its pseudocapacitive behavior, low cost and environmental benignity.[12,13] Ferrite, Fe_3O_4 with spinel structure, was shown to exhibit different capacitive behavior depending on the nature of aqueous electrolytes such as sulfite, sulfate, chloride, phosphate and hydroxide.[14,15] In a similar way, it has been reported that some crystalline ferrites with spinel structure, MFe_2O_4 [M = Mn, Fe, Co and Ni], exhibit pseudocapacitance in aqueous solutions of chlorides and sulfates of alkali/alkaline earth metals and organic electrolytes.[16–18] Among these ferrites, $MnFe_2O_4$ exhibited a pseudocapacitive behaviour whereas very low electrical double layer capacitance (EDLC) was observed with other ferrites.[16]

Spinels have the general formula of $[A]_{Td}[B_2]_{Oh}O_4$ [A = Na, Ag, Mg, Mn, Fe, Co, Ni, etc. and B = Al, Fe, W, Mo, etc.] and the unit cell contains 32 O-atoms in a cubic close packing arrangement with 8 tetrahedral (Td) and 16 octahedral (Oh) sites for the metal ions to occupy.[19] Spinel ferrites, MFe_2O_4, are potential materials with various electronic and magnetic applications.[20] $NiFe_2O_4$ is an inverse spinel in which Ni^{2+} occupies the octahedral site and half of the Fe^{3+} ions occupy the tetrahedral site. Thus, the compound can be represented by the formula $[Fe^{3+}]_{Td}[Ni^{2+}Fe^{3+}]_{Oh}O_4$.[19] $NiFe_2O_4$ has been widely employed in technological applications including satellite communications, memory devices, computer components, antenna rods and transformer cores due to its magnetic properties.[21] With its low microwave loss, magnetic anisotropy and magnetostriction behaviour, $NiFe_2O_4$ is being used in radio frequency/microwave applications.[22] Among the ferrites, $NiFe_2O_4$ is an interesting candidate to investigate as it contains electrochemically active nickel. It will be of fundamental interest to study the electrochemical properties of spinels as their properties depend on the structure and morphology. Obtaining an enhanced capacitance by optimizing the morphology of $NiFe_2O_4$ is of worth investigating. With this view, in the present study, we evaluated the electrochemical capacitive behavior of $NiFe_2O_4$ synthesized by adopting different synthetic strategies and established the morphology – property correlation.

Experimental

Synthesis.—The reagents used in the synthesis were $Ni(NO_3)_2.6H_2O$ (Merck, 99%), $Fe(NO_3)_3.9H_2O$ (Merck, 99%), glycine (Merck, 99%), alanine (Merck, 99%), diethylene glycol (DEG; SISCO Research Laboratories, 99.9%), ammonia solution (25%, Merck), 1-butanol (SISCO Research Laboratories, 99.5%) and glacial acetic acid (SISCO Research Laboratories, 99.9%). $NiFe_2O_4$ was synthesized by adopting different synthesis methods namely, combustion, polyol-mediated and sol-gel methods which are described below:

Combustion synthesis.—$NiFe_2O_4$ was synthesized using either glycine or alanine as a fuel. In a typical synthesis, stoichiometric quantities of oxidizer $Ni(NO_3)_2.6H_2O$ and $Fe(NO_3)_3.9H_2O$ and a fuel (glycine or alanine) were dissolved in minimum amount of water. The solution was stirred for ~3 h to get a homogeneous mixing of the reagents and then slowly heated at 100°C to get a viscous material. The obtained viscous dark brown material was introduced into a preheated muffle furnace that was kept around 450°C. Within few minutes, a very vigorous reaction took place with intense flame by decomposition of precursor liberating gases and finally a fluffy solid mass was obtained. Subsequently, this material was post annealed at 1000°C for 5 h to obtain a phase pure material.

Polyol-mediated synthesis.—$NiFe_2O_4$ was synthesized by polyol-mediated method using DEG. Stoichiometric amounts of $Ni(NO_3)_2.6H_2O$ and $Fe(NO_3)_3.9H_2O$ were dissolved in 100 ml DEG. A clear dark brown solution was obtained. Aqueous NH_3 was slowly added to adjust the pH to a value close to 12. The solution was rapidly heated to ~180°C and the stirring was continued. Particles were formed during heating. The solution was kept at 180°C for 1 h and then allowed to cool down to room temperature (RT)

* Electrochemical Society Active Member.
z E-mail: nlnsimha@gmail.com; laksnarasimhan@cecri.res.in

with constant stirring. After cooling to RT, 100 ml ethanol was added and stirred for 30 min. The formed particles were collected by centrifugation. The particles were washed with ethanol (~200 ml) and centrifuged. The obtained particles were dried at 100°C in an air oven for 8 h. The collected particles were heated at 1000°C for 5 h in a muffle furnace to obtain phase pure $NiFe_2O_4$.

Sol-gel synthesis.—In a typical synthesis, stoichiometric amounts of $Ni(NO_3)_2.6H_2O$ and $Fe(NO_3)_3.9H_2O$ were separately dissolved in solutions containing 15 ml 1-butanol and 5 ml glacial acetic acid. The two solutions were ultrasonicated for 30 min. Then $Fe(NO_3)_3.9H_2O$ solution in 1-butanol was added dropwise into the Ni-precursor solution under constant stirring. Then the solution was slowly heated to 120°C at which a brownish black gel was obtained which on further increase in temperature changed into a dry mass. The obtained mass was thoroughly ground and heated at 600°C for 5 h to get the oxide. The precursor was also heated at 1000°C for 5 h in order to make our comparison valid with the other samples that were heated at 1000°C.

Characterization.—The thermogravimetric and differential thermal analysis (TG-DTA) of the dried precursors of $NiFe_2O_4$ obtained by polyol-mediated and sol-gel methods were carried out using thermal analyzer (TA instrument, SDT Q600) in order to determine the decomposition and crystallization temperature. These experiments were carried out in air between 30 and 800°C at a heating rate of 10°C/min. The phase formation and purity were examined by powder X-ray diffraction (XRD) using Cu-Kα (1.5425 Å) radiation (D8, Advance, Bruker). The morphology of sintered $NiFe_2O_4$ samples was observed by scanning electron microscopic (SEM) technique (S-3000H, Hitachi). The FT-IR spectra of all four $NiFe_2O_4$ samples were recorded in the mid-IR region using KBr pellet technique (Tensor 27, Bruker). The Brunauer-Emmett-Teller (BET) surface area values of all four $NiFe_2O_4$ samples were measured by N_2 adsorption (Autosorb-IQ, Quantachrome). Cyclic voltammetry (CV) experiment was carried out in a three electrode assembly using a potentiostat-galvanostat (PG30, Autolab). A Pt foil (1.1×1.1 cm^2), a Pt rod and saturated calomel electrode (SCE) were used as a working, a counter and a reference electrode, respectively. The working electrode was prepared by mixing the active material $NiFe_2O_4$ (5 mg) with a conductive additive, activated carbon (AC; 25 mg) using a diluted Naffion solution. The mixture was ultrasonicated for 10 min and the obtained paste was coated over the Pt foil electrode using a brush. The coated electrode was dried at 100°C for 1 h and used as the working electrode. The CV experiments were carried out in the potential window of 0.0 to +0.8 V (*vs*. SCE) using NaCl (0.1 M) solution as the electrolyte.

Results and Discussion

Thermal analysis.—The TG–DTA of the precursors obtained in the polyol-mediated and sol-gel methods was carried out in order to confirm the complete removal of the organics used in the synthesis and the results are shown in Fig. 1. In the TG-DTA curve of the precursor obtained in the polyol-mediated method (Fig. 1a), a steep weight loss (28%) is observed between 97 and 200°C and this could be attributed to the removal of surface bound water and ethanol. The weight loss observed in the region between 240 and 300°C in the TGA curve and the exothermic peak at 261°C in the DTA curve could be attributed to the loss of residual DEG molecules as the boiling point of DEG is 244–245°C. This result shows that the precursor obtained in the polyol-mediated method consists of residual DEG molecules over the surface and this is due to the incomplete removal of DEG by washing with ethanol. In polyol-mediated synthesis, the DEG not only acts as a solvent but also acts as a capping agent in stabilizing the nanoparticles from random agglomeration.[23] This exothermic peak could also be due to the crystallization of $NiFe_2O_4$. No weight loss was observed after 356°C. Similarly the TG-DTA curve of the precursor obtained by sol-gel method (Fig. 1b) exhibited a total weight loss of 50% by heating it from 30 to 300°C. The weight loss in the initial stages is very gradual up to 200°C beyond which a major weight loss is observed till 300°C. In this case, there could be organics and residual nitrates in the sample as no washing was employed in the synthesis. There is an exothermic peak in the DTA curve at 292°C which could be due to the crystallization of $NiFe_2O_4$ as observed in the case of polyol-mediated method in Fig. 1a. These results reveal the complete decomposition of precursors obtained in both polyol-mediated and sol-gel methods by heating them up to 400°C in air beyond which there is no weight loss indicating the formation of oxide.

Phase formation.—The powder XRD patterns of $NiFe_2O_4$ obtained by different synthesis routes are shown in Fig. 2 along with the standard pattern available in the data base of joint committee on powder diffraction standards (JCPDS 10-0325). In all cases, the samples were calcined at 1000°C in air. We chose this temperature since a small amount of unidentified phase was observed along with $NiFe_2O_4$ obtained by combustion synthesis using glycine as a fuel and a single phase was obtained by annealing at 1000°C (data not shown). The crystallinity was shown to be an important parameter to have a large capacitance value in the case of $MnFe_2O_4$.[16] On the other hand, a single phase $NiFe_2O_4$ was obtained by heating the precursor from sol-gel method at 600°C for 6 h. Since our aim is to compare the electrochemical capacitance behavior of $NiFe_2O_4$

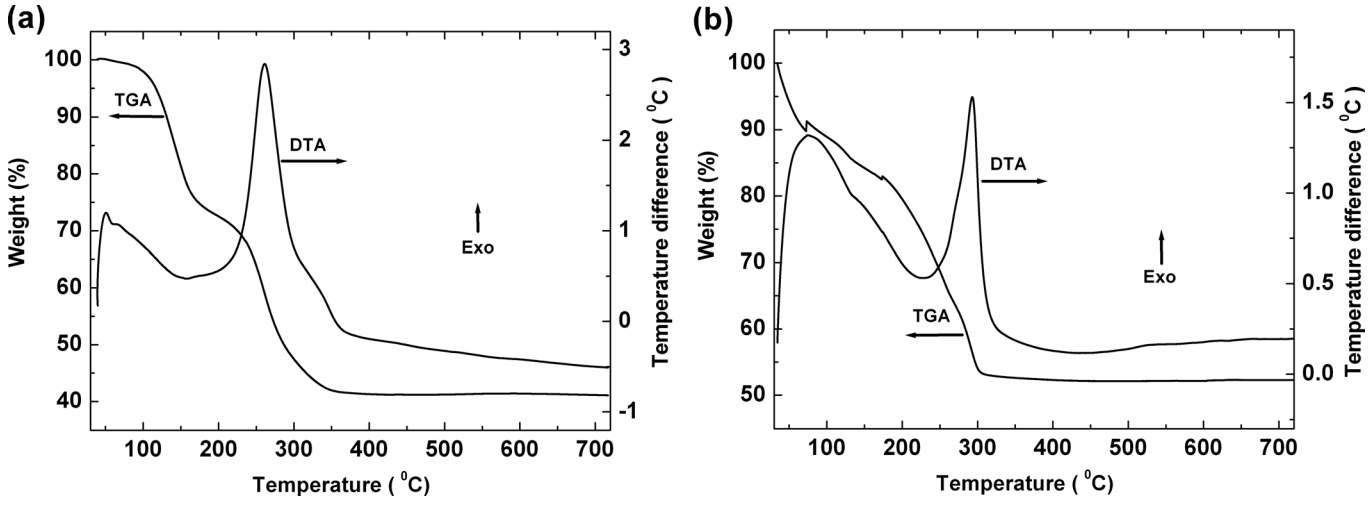

Figure 1. TG-DTA curves of dried precursors of $NiFe_2O_4$ obtained by (a) polyol-mediated and (b) sol-gel methods.

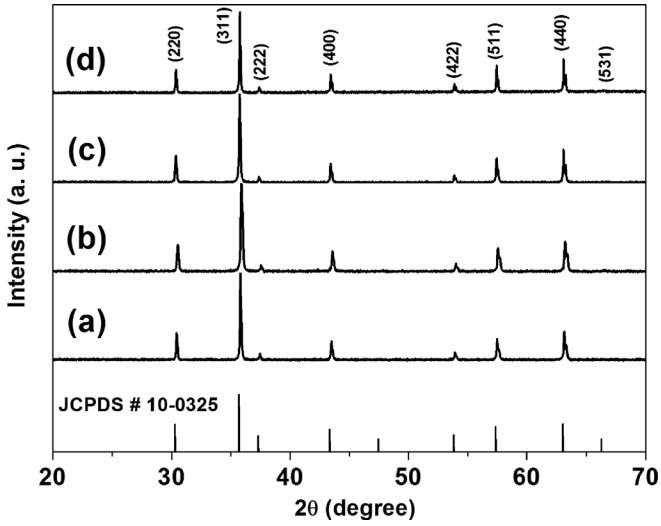

Figure 2. Powder XRD patterns of $NiFe_2O_4$ synthesized by (a and b) combustion method using glycine and alanine as fuels, respectively, (c) polyol-mediated method and (d) sol-gel method. The standard pattern of $NiFe_2O_4$ is for comparison (JCPDS # 10-0325).

synthesized by different methods, we calcined all samples at 1000°C to make our comparison a more realistic one.

The powder XRD patterns of $NiFe_2O_4$ obtained by different methods are identical in nature and reveal the formation of cubic $NiFe_2O_4$ as compared with the standard pattern shown in Fig. 2. All the reflections were indexed based on the standard. The absence of any noticeable diffraction peaks of other impurities reveals the formation of a single phase. The cubic lattice parameters were determined by Rietveld profile-matching method using FullProf program.[24,25] The calculated cubic lattice parameter values in all four samples are almost same [8.340(1) Å] which are in good agreement with the value of the standard $NiFe_2O_4$ (8.339 Å).

Morphological analysis.—The morphologies of $NiFe_2O_4$ synthesized through different methods were analyzed by SEM and the images are shown in Fig. 3. SEM images show that the ferrite powders contain uneven morphology consisting of a large smooth area with no evidence of any intergranular phase(s). $NiFe_2O_4$ prepared by combustion synthesis (Figs. 3a and 3b) exhibits a network with voids and pores formed by the escaping gases during the combustion reaction. There are large agglomerates without any clear grain boundaries. This type of agglomeration is typical of combustion synthesized powders.[26,27] In the case of $NiFe_2O_4$ obtained by polyol-mediated method, the particles were smaller when compared to the sample prepared by combustion synthesis. However, these small particles are randomly agglomerated and there is no uniform shape of particles observed. The morphology of $NiFe_2O_4$ synthesized by sol-gel method resembles that of sample obtained by combustion synthesis, i.e., the agglomerates with pores formed in between them. In the sol-gel sample, the agglomerates are smaller in size when compared to the samples obtained by combustion synthesis. The pores or voids formed with the sol-gel sample are better than the ones formed with the samples obtained by combustion synthesis. Thus, the difference in the morphologies of $NiFe_2O_4$ synthesized by different methods may influence the electrochemical capacitance properties as the EDLC originates from the accumulation and building up of charges within the pores of a material.

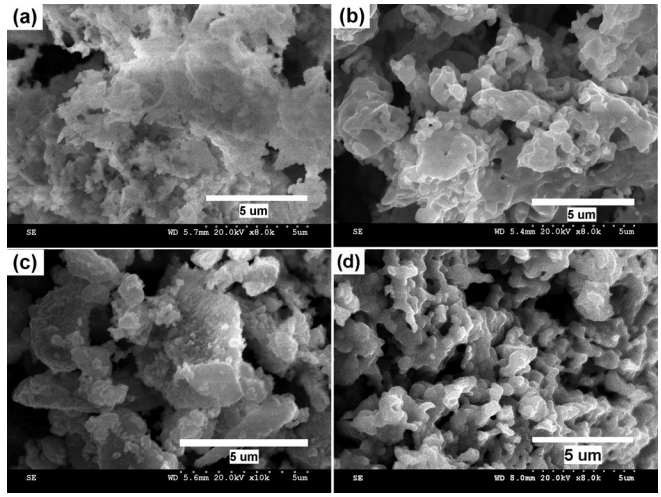

Figure 3. Scanning electron micrographs of $NiFe_2O_4$ obtained by (a and b) combustion synthesis using glycine and alanine as fuels, respectively, (c) polyol-mediated method and (d) sol-gel method.

FT-IR spectroscopic analysis.—The FT-IR spectrum of $NiFe_2O_4$ synthesized by combustion synthesis using glycine as a fuel is shown in Fig. 4 and the spectra of all samples synthesized by other methods resembled the same. In spinels, it has been observed that the stretching vibrations of the metal oxygen bonds occur in the range between 600 and 550 cm^{-1} for the metal ion occupying the tetrahedral site whereas the stretching vibration of the metal ion in the octahedral site occurs in the range 450–385 cm^{-1}.[28] Accordingly in the spectrum of $NiFe_2O_4$ (Fig. 4), we assign the broad band with the absorption maximum at 596 cm^{-1} to the tetrahedral site Fe-O stretching vibration since $NiFe_2O_4$ is an inverse spinel in which half of Fe occupies the tetrahedral site and the narrow band observed at 402 cm^{-1} to the stretching vibration of metal (Fe and/or Ni) oxygen bond at the octahedral site.[29] The absence of any other additional absorption reveals the phase purity of the synthesized samples.

Electrochemical properties.—CV was used to evaluate the electrochemical capacitive behaviour of $NiFe_2O_4$ synthesized through various routes. An aqueous solution of 0.1 M NaCl was used as an electrolyte and the electrochemical characteristics were investigated over a potential range from 0.0 to 0.8 V *vs*. SCE at different potential sweep rates. Figure 5 shows the CV curves of $NiFe_2O_4$–AC composite electrodes in 0.1 M NaCl aqueous solution at a potential scan rate of 2 mV/s. Two characteristic features can easily be noted from these CVs. First, the current–potential profiles exhibit nearly a rectangular shaped voltammogram, suggesting a true

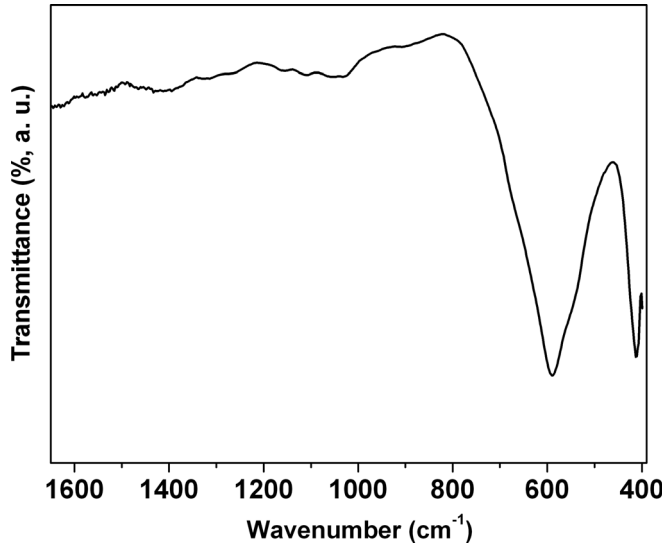

Figure 4. FTIR Spectrum of $NiFe_2O_4$ obtained by combustion synthesis using glycine as a fuel.

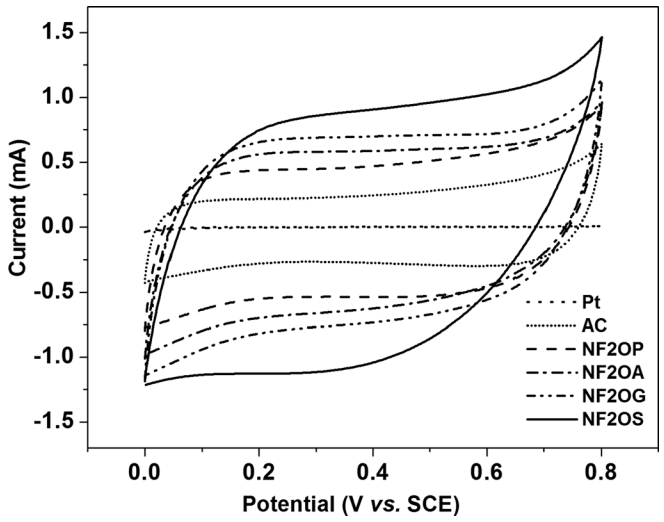

Figure 5. Cyclic voltammograms of $NiFe_2O_4$ obtained by different methods: combustion synthesis using glycine and alanine as fuels (NF2OG and NF2OA, respectively), polyol-mediated method (NF2OP) and sol-gel method (NF2OS). The CVs of bare Pt electrode and carbon coated Pt electrode are also shown for comparison. The scan rate is 2 mV/s and the electrolyte is 0.1 M aqueous NaCl.

electrochemical capacitive behavior over the entire potential range used in the study. Secondly, the current observed in the case of a current collector (Pt foil) is very negligible when compared to that of AC and AC-$NiFe_2O_4$ coated electrodes. From the CV results it is clearly evident that $NiFe_2O_4$ exhibits higher current compared to that of bare Pt and AC suggesting that $NiFe_2O_4$ samples synthesized using all the four methods are electrochemically active. It can also be seen from these CV profiles that the addition of $NiFe_2O_4$ to AC results in a 3-fold increase in the current of pure AC. Though $NiFe_2O_4$ consists of transition metal ions which can undergo facile redox reactions ($Ni^{2+/3+}$ and/or $Fe^{3+/2+}$), we did not observe any such result (peak formation) in these CVs indicating the absence of pseudocapacitive behavior. This result is in agreement with the literature report of MFe_2O_4 [M = Mn, Fe, Co and Ni] among which only $MnFe_2O_4$ exhibited a pseudocapacitive behavior whereas the other ferrites showed only EDLC behaviour.[16] This difference has been attributed to the site occupancy of the divalent transition metal ions in the spinel crystal structure. $MnFe_2O_4$ has a normal spinel structure and the others have an inverse spinel structure.[16,19] The divalent metal ions in the tetrahedral site alone exhibit the pseudocapacitive behavior whereas the same ions in octahedral site do not. In $NiFe_2O_4$, Ni^{2+} occupies the octahedral site and hence no signature of its redox behavior is observed in the CV results of $NiFe_2O_4$ obtained by four different methods in the present study (Fig. 5). Thus, the observed electrochemical behavior is only of EDLC and not of the pseudocapacitive. In the normal spinel structure, the divalent metal ion is in the tetrahedral site which is isolated in the structure from other tetrahedral sites. On the other hand, if the divalent metal ion occupies the octahedral site in inverse spinel, they are connected to other divalent and trivalent ions in the 3-dimensional network structure. Hence, the electronic conduction by electron (or hole) hopping is facile in the octahedral sites.[14] Thus, they do not exhibit any pseudocapacitive behavior. The EDLC values were calculated from the CVs shown in Fig. 5 using the following equation:[5]

$$C = I_a + I_c/(2 \times \ \nu)$$

where C is the double layer capacitance in F/cm^2, I_a and I_c are the current values of anodic and cathodic regions, respectively, measured at a constant potential of 0.4 V (*vs.* SCE) and ν is the scan rate.

Table I summarizes the current density, capacitance and specific capacitance values determined for various electrodes. From Table I, it can easily be noted that $NiFe_2O_4$ synthesized using sol-gel method exhibits a higher specific capacitance value compared to all the other electrodes studied in this work. AC provides a double layer capacitance of 0.106 F/cm^2, which corresponds to a specific capacitance of 4.3 F/g. On the other hand, $NiFe_2O_4$ prepared using various methods exhibited a higher EDLC. Among them the sample prepared through sol-gel route has shown a maximum specific capacitance of 97.5 F/g. The difference in the capacitance values arises mainly from the method adopted for the synthesis and the resultant morphology. The change in specific capacitance values follows the order of synthesis methods: *polyol<combustion (alanine)<combustion (glycine)<sol-gel*. This effect can easily be visualized from Figs. 5 and 6, which display the CVs and change in specific capacitance values with respect to scan rate. The measured BET surface areas are 1.624, 0.747, 3.049 and 0.968 m^2/g for $NiFe_2O_4$ obtained by combustion (glycine), combustion (alanine), polyol and sol-gel methods, respectively. The observed low surface areas are mainly due to the annealing of samples at 1000°C which also results in the rupture of porous structures. We could not find any direct relation between the specific capacitance and surface area of $NiFe_2O_4$ samples in the present study. There could be other possible reasons for this. In all the electrochemical experiments, $NiFe_2O_4$ was mixed with AC and hence its effective surface area used to observe the EDLC behavior may not be the same as the one measured by BET method. The mixing of active material with AC may modify the surface area. It has been observed that a well balanced micro- and mesoporosity of the

Table I. The calculated current density, double layer capacitance and specific capacitance values from the CVs (Fig. 5) of $NiFe_2O_4$ synthesized by combustion synthesis using glycine and alanine as fuels (NF2OG and NF2OA, respectively), polyol-mediated method (NF2OP) and sol-gel method (NF2OS).

Sample	Current density (mA/cm^2)	Capacitance (F/cm^2)	Specific capacitance (F/g)
AC	0.213	0.106	4.3
NF2OG	0.591	0.295	71.5
NF2OA	0.504	0.252	61.0
NF2OP	0.417	0.208	50.5
NF2OS	0.805	0.403	97.5

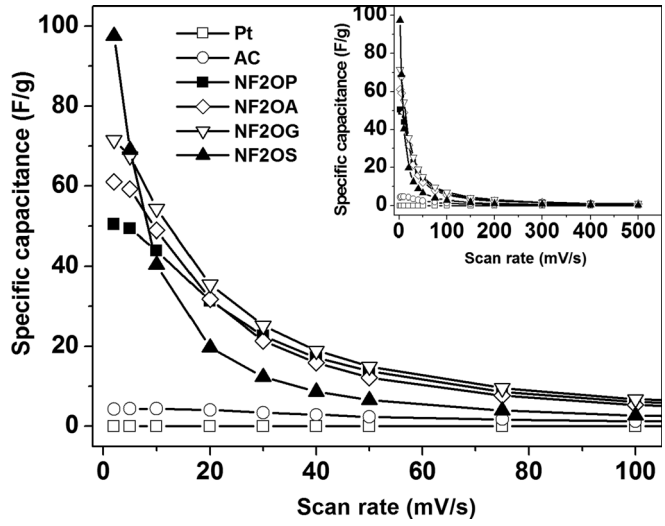

Figure 6. The variation in calculated specific capacitance values of $NiFe_2O_4$ obtained by different methods: combustion synthesis using glycine and alanine as fuels (NF2OG and NF2OA, respectively), polyol-mediated method (NF2OP) and sol-gel method (NF2OS) with respect to scan rate. The values are calculated from the CV data shown in Fig. 5. The inset showing the specific capacitance data obtained over the entire scan rate range upto 500 mV/s.

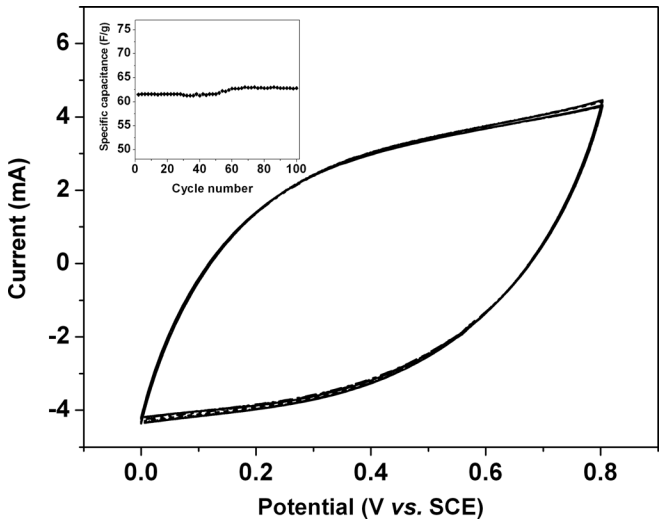

Figure 7. Cyclic voltammograms of $NiFe_2O_4$ (solgel)-AC composite electrode in aqueous NaCl solution (0.1 M) at a scan rate of 5 mV/s. The inset shows the variation in calculated specific capacitance with respect to cycle number.

electrode material is necessary to achieve a higher capacitance.[6] It is known in the case of carbon that the specific capacitance has a linear dependence on the surface area in the low surface area region and reaches a plateau when the surface area increases.[7] Hence, the variation in the EDLC values among the four $NiFe_2O_4$ samples can be attributed to the difference in their morphologies which in turn depends on the synthetic strategy adopted.

Several methods such as co-precipitation, hydrothermal, sol–gel, combustion synthesis, etc. have been successfully employed in the synthesis of $NiFe_2O_4$.[30–33] Among the various methods, the combustion synthesis is a rapid one to prepare simple binary and ternary ferrites.[34] The sol-gel method is advantageous in obtaining monodispersed powders and multicomponent ceramics and the morphologies can be fine tuned by varying the experimental conditions.[35] Polyol-mediated method has recently been emerged as a promising method for the synthesis of nanoparticles in which multidendate alcohols are used both as solvent and capping agent to control the size of the particles.[23] In the present study, we find that the four different methods led to the different morphologies of $NiFe_2O_4$. Though the polyol-mediated method resulted in a combination of smaller and larger particles (Fig. 3c), they are not connected to each other. Such irregularity in the particle size and poor connectivity among the particles may be the reason for the observed lowest specific capacitance value for $NiFe_2O_4$ synthesized by polyol-mediated method when compared to the values obtained with the other samples. In the case of combustion synthesis which resulted in porous materials, there are no clear grain boundaries with the sample obtained using glycine as a fuel. Though $NiFe_2O_4$ synthesized by combustion synthesis (using alanine as a fuel) and sol-gel method exhibit a close resemblance in their morphologies (Figs. 3b and 3d), the grains and pores are smaller with $NiFe_2O_4$ obtained by sol-gel method and this may well be the reason for the highest specific capacitance value obtained with this sample among all other samples. Our results indicate that the inter-particle or inter-grain connectivity within the aggregate is important for the charge transfer process in addition to the porous structure.

Figure 6 shows the plot of variation of specific capacitance with the scan rate for all the electrodes used in our study. The inset in Fig. 6 displays the same plot for the entire range of scan rate used. The specific capacitance values were found to increase exponentially with decreasing the scan rate and this observation is attributed to increasing ionic resistance within the pores. It can be seen from Fig. 6 that in the case of Pt foil and AC electrodes the change in specific capacitance values with scan rate is negligible. On the contrary, $NiFe_2O_4$ prepared using combustion (alanine and glycine as fuels) and polyol-mediated methods provide a two-fold decrease in the capacitance values for an order of change in the scan rate except for $NiFe_2O_4$ prepared using sol-gel method where the decrease was found to be higher. Investigating the effect of scan rate on specific capacitance values provides valuable information on the rate of discharge of these electrodes. It has been found that the specific capacitance of $NiFe_2O_4$ prepared using sol-gel method decays faster compared to $NiFe_2O_4$ obtained by combustion and polyol-mediated methods suggesting the higher rate of discharge at the interface. This implies a fast response time for the device when $NiFe_2O_4$ (sol-gel method) is used as an electroactive capacitor. Nevertheless, the highest specific capacitance value was obtained in the case of $NiFe_2O_4$ synthesized using sol-gel method. In order to find the stable performance of $NiFe_2O_4$ electrode, we performed the cycle stability test in the single electrode configuration that was used in all our experiments. The cycle test was carried out with $NiFe_2O_4$ obtained by sol-gel method as it exhibited the higher specific capacitance when compared to other three samples and the results are shown in Fig. 7. We could find a stable performance of the electrode as there is no major change in the CVs (even for more than 100 cycles at different scan rates) and almost a stable specific capacitance value has been obtained (inset in Fig. 7). From this result we could confirm the stable EDLC behaviour of $NiFe_2O_4$ electrode.

We also investigated the effect of potential range on the EDLC behaviour of these $NiFe_2O_4$ electrodes. A wide potential range was employed for the study and the corresponding CVs are displayed in Fig. 8. The CV profiles may easily be misinterpreted for the indication of equivalent series resistance (ESR), but careful examination of these CVs suggests that it is not the case. It can be seen from Fig. 8 that upon reversing the potential scans the response current due to double layer charging is very fast at both the ends, indicating a smaller value of ESR in the present case. This is also supported by the higher values of specific capacitance obtained for the present system. Accordingly, the CV profiles exhibit a strong potential dependence on the specific capacitance. The obtained highest specific capacitance of $NiFe_2O_4$ (sol-gel method) could be attributed mainly to surface area, easy accessibility of ions through pores and well connected grains. Recently, an enhancement in the discharge capacitance of $NiFe_2O_4$ has been demonstrated by forming a composite with PEDOT.[36] From our results we infer that $NiFe_2O_4$ is a potential material for electrochemical capacitor applications and further optimization of uniform porous network structure, making a composite

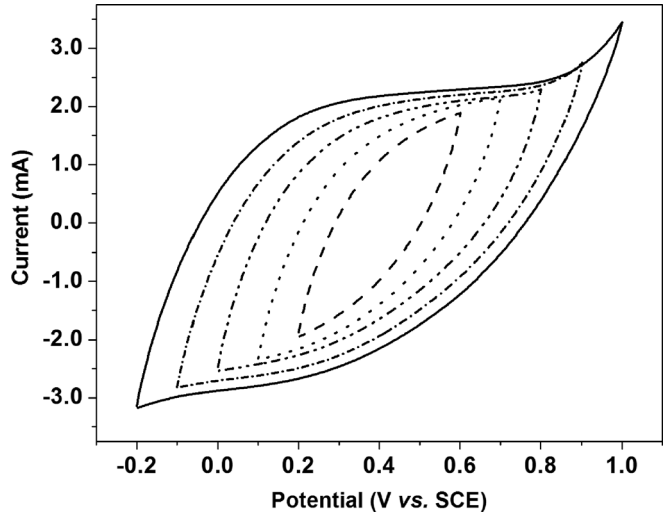

Figure 8. Cyclic voltammograms of $NiFe_2O_4$ synthesized by sol-gel method in 0.1 M aqueous NaCl solution in different potential window with the scan rate of 5 mV/s.

and a proper choice of electrolyte may increase the performance of this material.

Conclusions

$NiFe_2O_4$ was synthesized by adopting different synthetic strategies such as combustion, polyol-mediated and sol-gel methods. The phase formation and morphologies of the synthesized materials were characterized and it was found that the morphology depends on the synthesis method. The electrochemical property was investigated in aqueous NaCl solution (0.1 M) using CV and the results reveal the electrochemical double layer capacitive behavior of $NiFe_2O_4$. Our results demonstrate a high specific capacitance value of 97.5 F/g suggesting its potential application as a capacitor. The enhanced capacitance of $NiFe_2O_4$ has been found to originate from the porous structure and well interconnected nanoparticle morphology.

Acknowledgments

The author KSM acknowledges the Council of Scientific and Industrial Research (CSIR), New Delhi for a research assistantship through CSIR-Diamond Jubilee Research Intern program. Central Instrumentation Facility (CIF) of CSIR-CECRI is acknowledged for characterization facilities. CSIR-Institute of Minerals and Materials Technology, Bhubaneswar is acknowledged for BET surface area measurement. The work was financially supported by CSIR Non-Network Project (No. OLP 0054).

References

1. B. E. Conway, *J. Electrochem. Soc.*, **138**, 1539 (1991).
2. A. K. Shukla, S. Sampath, and K. Vijayamohanan, *Curr. Sci.*, **79**, 1656 (2000).
3. R. Kötz and M. Carlen, *Electrochim. Acta*, **45**, 2483 (2000).
4. V. L. Pushparaj, M. M. Shaijumon, A. Kumar, S. Murugesan, L. Ci, R. Vajtai, R. J. Linhardt, O. Nalamasu, and P. M. Ajayan, *Proc. Natl. Acad. Sci.*, **104**, 13574 (2007).
5. B. E. Conway, *Electrochemical Supercapacitors: Scientific Fundamentals and Technological Applications*, Kluwer Academic/Plenum Publishers, New York (1999).
6. P. Simon and Y. Gogotsi, *Nature Mater.*, **7**, 845 (2008).
7. P. Simons and A. C. Burke, *Electrochem. Soc. Interface*, **17**, 38 (2008).
8. J. P. Zheng and T. R. Jow, *J. Electrochem. Soc.*, **142**, L6 (1995).
9. A. Rudge, J. Davey, I. Raistrick, and S. Gottesfeld, *J. Power Sources*, **47**, 89 (1994).
10. J. P. Zhang, P. J. Cygan, and T. R. Jow, *J. Electrochem. Soc.*, **142**, 2699 (1995).
11. H. Y. Lee and J. B. Goodenough, *J. Solid State Chem.*, **144**, 220 (1999).
12. K.-C. Liu and M. A. Anderson, *J. Electrochem. Soc.*, **143**, 124 (1996).
13. V. Ganesh, V. Lakshminarayanan, and S. Pitchumani, *Electrochem. Solid State Lett.*, **8**, A308 (2005).
14. N.-L. Wu, S.-Y. Wang, C.-Y. Han, D.-S. Wu, and L.-R. Shiue, *J. Power Sources*, **113**, 173 (2003).
15. S.-Y. Wang and N.-L. Wu, *J. Appl. Electrochem.*, **33**, 345 (2003).
16. S.-L. Kuo and N.-L. Wu, *Electrochem. Solid-State Lett.*, **8**, A495 (2005).
17. S.-L. Kuo and N.-L. Wu, *Electrochem. Solid State Lett.*, **10**, A171 (2007).
18. S.-L. Kuo, J.-F. Lee, and N.-L. Wu, *J. Electrochem. Soc.*, **154**, A34 (2007).
19. F. Wells, *Structural Inorganic Chemistry*, 3rd ed., Oxford University, London (1962).
20. S. Anjum, G. H. Jaffari, A. K. Rumaiz, M. S. Rafique, S. I. Shah, and *J. Phys. D: Appl. Phys.*, **43**, 265001 (2010).
21. M. A. F. Ramalho, L. Gama, S. G. Antonio, C. O. Paiva-Santos, E. J. Miola, R. H. G. A. Kiminami, and A. C. F. M. Cost, *J. Mater. Sci.*, **42**, 603 (2007).
22. X. Zuo, S. Yan, B. Barbiellini, V.G. Harris, and C. Vittoria, J. Magn. Magnetic Mater., **303**, e432 (2006).
23. C. Feldmann and H. O. Jungk, *Angew. Chem. Int. Ed.*, **40**, 359 (2001).
24. R. A. Young, in *The Rietveld Method*, Oxford University, Oxford (1995).
25. J. Rodríguez-Carvajal, An Introduction to the Program FullProf 2000 (2001).
26. T. Striker and J. A. Ruud, *J. Am. Ceram. Soc.*, **93**, 2622 (2010).
27. H. Kavas, N. Kasapoğlu, A. Baykal, and Y. Köseoğlu, *Chem. Papers*, **63**, 450 (2009).
28. R. D. Waldron, *Phys. Rev.*, **99**, 1727 (1955).
29. M. A. Gabal, *J. Phys. Chem. Solids*, **64**, 1375 (2003).
30. A. H. Morr and K. Haneda, *J. Appl. Phys.*, **52**, 2496, (1981).
31. S. Komarneni, E. Fregeau, E. Breval, and R. Roy, *J. Am. Ceram. Soc.*, **71**, c–26, (1998).
32. P. Courty, H. Ajot, C. Macilly, and B. Delmon, *Powder Technol.*, **7**, 21, (1973).
33. S. Prasad and N. S. Gajbhiye, *J. Alloys Compds.*, **265**, 87, (1998).
34. K. C. Patil, S. T. Aruna, and S. Ekambaram, *Curr. Opin. Solid State Mater. Sci.*, **2**, 158, (1997).
35. J. Livage, M. Henry, and C. Sanchez, *Prog. Solid State Chem.*, **18**, 259 (1988).
36. P. Sen and A. De, *Electrochim. Acta*, **55**, 4677 (2010).